Full phase and amplitude control in computer generated holography

Markus Fratz*,1,2, Peer Fischer2, Dominik M. Giel1

1Fraunhofer Institute for Physical Measurement Techniques IPM, Heidenhofstrasse 8, 79110 Freiburg, Germany
2 Rowland Institute at Harvard, Harvard University, 100 Edwin H. Land Boulevard, Cambridge, Massachusetts 02142, USA
* Corresponding author: markus.fratz@ipm.fraunhofer.de

We report the first realization of a computer generated complex-valued hologram recorded in a single film of photoactive polymer. Complex-valued holograms give rise to a diffracted optical field with control over its amplitude and phase. The holograms are generated by a novel one-step direct laser writing process in which a spatial light modulator (SLM) is imaged onto a polymer film. Temporal modulation of the SLM during exposure controls both the strength of the induced birefringence as well as the orientation of the fast axis. We demonstrate that the complex holograms can be used to impart arbitrary amplitude and phase profiles onto a beam and thereby open new possibilities in the control of optical beams.

Simultaneous control of both the amplitude and the phase distribution across a diffracted light beam has been a longstanding aim of computer generated holography [1] and would permit the efficient generation of e.g non-diffracting beams or airy beams [2, 3], optical traps [2, 4] or three-dimensional displays [5]. To date computer generated holograms (CGH) only control either the phase or the amplitude separately. No direct method to generate complex holograms exists, but several workarounds have been developed. These include multi-emulsion films (separate phase and amplitude holograms sandwiched together [6]), or sophisticated numerical methods based on either a pure phase [7] or a pure amplitude [8] hologram to approximate a true complex-valued hologram. CGHs calculated by these approximate methods exhibit a number of drawbacks: First, their fabrication is more demanding as they require additional high-resolution grating structures (HRGS) to generate the high frequency spatial components for these pseudo-complex CGHs. Second, their application is limited to optical systems where the higher diffraction orders introduced by the HGRS can be filtered out so that free-space application of such holograms is impossible. Third, the introduction of the HRGS limits the spatial frequency and thereby the resolution of the hologram. CGHs that control amplitude and phase directly would not suffer from these drawbacks and would, moreover, allow the perfect reconstruction of arbitrary wave fields while having a superior suppression of speckle. Speckle in diffractive optics arises from the random phase distribution of the diffracted field that has to be applied to achieve a particular intensity distribution [9]. If amplitude and phase of the CGH are controlled, the random phase distribution can be omitted resulting in a reduction of the speckle pattern.

The theory of complex-valued CGHs with polarization control has been discussed previously [10]. We have recently shown [11] how phase and amplitude can be controlled independently in a polarization hologram to allow the storage of two independent images in a single hologram. In this Letter, we demonstrate a more efficient writing technique for polarization holography with orders of magnitude higher write speeds and also show how a complex hologram can be used to generate free-space beams with complex beam profiles defining both the amplitude and the phase of the beam.

The holograms are written in a polymer that contains two side-groups. One is a photo-active azobenzene dye-group that undergoes efficient *cis- trans-* isomerization under illumination of green (or shorter wavelength) light and the other is a liquid-crystal like side-chain that changes its alignment once the photo-active molecules are illuminated with linearly polarized light. This molecular orientation results in a linear birefringence [11, 12, 13]. The orientation of the induced birefringence can be controlled by the orientation of the polarization of the write laser beam. The optical anisotropy remains stable under illumination with light at wavelengths longer than the absorption of the dye. For the photo-polymer used in our experiments the birefringence can be observed with red light [14].

A layer of laterally varying birefringence acts as a hologram [12]. If it is illuminated by a left-circularly polarized beam $\sqrt{1/2}[1,i]^T$ and the direction and magnitude of the birefringence in any point of the layer is denoted by ρ and δ, respectively, then the (right-circularly) polarized component of the transmitted beam is given by [11,13]:

$$E_{out}^{rcp} = \frac{1}{\sqrt{2}} \sin\left(\frac{\delta}{2}\right) \cdot \exp\left(i\left(2\rho + \frac{\pi}{2}\right)\right) \cdot \begin{bmatrix} 1 \\ -i \end{bmatrix} \quad (1)$$

Thus, the amplitude of a transmitted beam depends on the magnitude of the induced birefringence δ while the phase is given by its rotation angle ρ. If it is possible to write structures in the polymer layer with defined δ and ρ, then CGHs controlling both amplitude and phase can be fabricated.

The setup for the generation of the CGHs is depicted in fig. 1. The write laser (L_1, wavelength = 532 nm, output

power = 30 mW) first passes a beam stop (BS) that is smaller than the laser beam diameter. The beam expanding optics (BEO) expands the laser and images
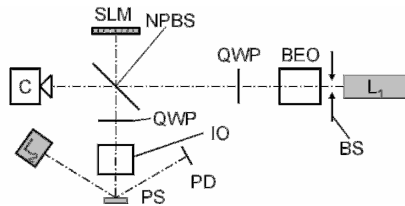

Fig. 1: Setup for the generation of amplitude and phase holograms. L_1: write laser (532 nm); BS: beam stop; BEO: beam expanding optics; NPBS: non-polarizing beam splitter; SLM: spatial light modulator; QWP: quarter-wave plate; IO: imaging objective; PS: polymer sample; C: Camera; L_2: control laser (670 nm); PD: photo diode

the beam stop into the plane of the spatial light modulator (HoloEye HEO1080P, pixel size 8 μm). LCD-based SLMs can control the polarization of the reflected beam if two quarter-wave plates (QWP) are used [15], illuminating the SLM with circularly polarized light. Each of the 1920 x 1080 pixels of the SLM introduces retardation on one component of the electric field of the write laser beam. The voltage applied to each pixel controls the retardation. After passing the SLM and the second QWP the polarization of the light in each pixel is linear, but the rotation angle of the linear polarization is defined by the voltage applied to each SLM-pixel [15]. The objective (IO, 10x microscope objective, NA 0.3) images the SLM onto the plane of the photo active polymer sample (PS). The nominal image size of each SLM-pixel is 0.8 μm in the plane of the PS, the diffraction limit of the objective is approx. 1 μm. To control the focus of the image of the SLM a CCD-Camera (C) is added to the setup. The PS is approx 2 μm thick and is spin-coated on an aluminum mirror. Each pixel of the SLM corresponds to a pixel of the hologram in the PS. Thus, the direction of the birefringence in each hologram pixel is defined by the voltage applied to the corresponding SLM-pixel. Upon illumination, the strength of the birefringence increases until the photo active molecules reach a maximum steady-state alignment. A measure of the induced anisotropy is the amount of light intensity that is diffracted into a first diffraction order, if for example a grating is written in the polymer. To measure this diffraction efficiency during hologram writing, a read-out laser L_2 (wavelength 670 nm) illuminates the hologram. The intensity of the first diffraction order is monitored using a photo diode (PD).

To record holograms with spatially varying amplitude, the SLM was used as a dynamically changing polarization mask. If the SLM image changes fast in comparison with the alignment process, then the polymer does not reach a high degree of alignment. By this method it is even possible to reduce or erase any previously -written anisotropy. A typical exposure is schematically depicted in fig. 2 (a). During the time T_S the SLM-pixel displays a static polarization mask and induces birefringence in the

polymer. During T_M the polarization direction generated by the SLM pixel is continuously oscillated which results in an effective reduction of the
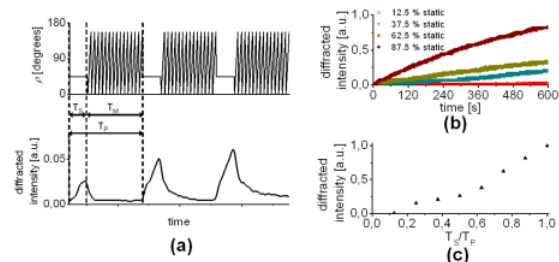

Fig. 2: Generation of gratings for different exposure times. (a) Time dependence of the polarization orientation ρ in a single SLM-pixel and measured diffracted intensity during the writing of a grating for a given time period in every pixel. T_S: time interval of static polarization; T_M time of modulation; period $T_P=T_S+T_M$ was chosen to be 120 s. (b) time dependent diffracted intensities for various ratios of T_S/T_P with $T_P \approx 5.3$ s during exposure. (c) diffracted intensities after 10 min exposure as a function of the T_S/T_P ratio

birefringence. The full period of a static-dynamic-cycle is denoted by T_P. A number of test gratings were first written into the polymer. For each grating the ratio T_S/T_P was set constant for all pixels of the SLM for each exposure. The diffracted intensity, normalized to the maximum value achieved for $T_S/T_P=1$, is depicted as a function of time and T_S/T_P is shown in fig. 2 (b) and (c), respectively. For $T_S/T_P=1$, maximum efficiencies of up to 50 % were achieved.

In summary, the amplitude and the phase of the diffracted beam are controlled by imaging a SLM into a photo-active polymer layer. The orientation of the polarization in a pixel during T_S defines the phase of the polarization hologram's pixel. The fraction of the time (T_S/T_P) during which the SLM displays static direction of polarization sets the amplitude.

The results of the fabrication of two example CGHs with binary amplitude and multi-level phase are given in fig. 3. The first has a ring-shaped amplitude distribution and a vortex phase that spans the range from 0 to 6π (wrapped from 0 to 2π) for one full revolution (fig. 3 a). For read-out with circularly polarized illumination (wavelength 643 nm), the hologram was inserted in a lensless digital holographic setup [16]. Three phase shifted interferograms at one wavelength were recorded approx. 140 mm behind the CGH [16]. One of the interferograms is depicted on top of fig. 3 (b). Numerical reconstruction of the phase and amplitude in the plane of the CGH yields the amplitude and phase image in the plane of the CGH. The results are in agreement with the target amplitude and phase images, as the ring-shaped amplitude and the circular phase with the three phase discontinuities are clearly observable. In a second CGH, a ring-shaped amplitude with the vortex phase spanning 0 to 8π was written. The holographic reconstructions are shown in fig. 3 (c). The circular amplitude and the spiral phase are clearly

seen, in particular the 4 phase discontinuities. Fig. 4 shows a CGH consisting of two regions with different
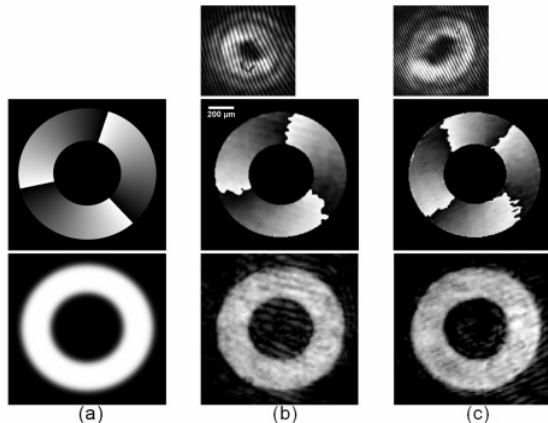

Fig. 3: CGHs with circular amplitude and spiral phase. (a) desired phase (top) and amplitude (bottom); (b) interferogram 140 mm behind CGH (spiral phase from 0 to 6 π) with tilted reference beam (top), reconstructed phase and amplitude in the plane of the CGH (scale bar is 200 µm); (c) interferogram (top), reconstructed phase and amplitude for CGH with a circular amplitude and spiral phase ranging from 0 to 8π

non-zero amplitudes and spiral phases with opposite sense of rotations. The desired amplitude and phase distributions are shown in fig. 4 (a). In fig. 4 (b) the amplitude and phase of the CGH fabricated in the PS are shown. Images were reconstructed using lensless digital holography. The two distinct regions are clearly
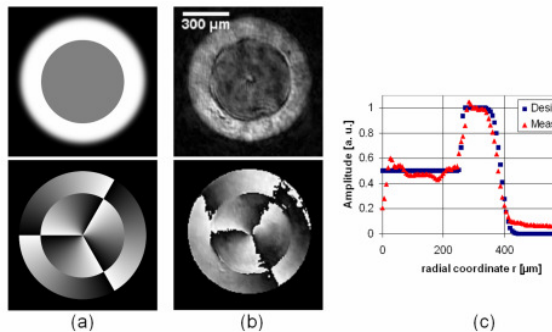

Fig. 4: CGH with two regions of different non-zero amplitude and changing spiral phase pattern with opposite sense of rotation. (a) Desired amplitude and phase. (b) Measured amplitude and phase using lensless digital holography. (c) Radial amplitude profile of the measured and desired amplitude (in arbitrary units).

observable both in the amplitude and the phase image and are in good agreement with the predicted distributions. Vortices with opposite sense of rotation are seen in the phase image. The rms error between the desired and measured phase distributions is 0.26 rad. From this value the number of resolvable phase values is estimated to be greater than 20. The radial profiles of measured and predicted amplitude distribution are shown in fig. 4 (c).The amplitude in the central region is 50% of the outer ring as intended. The rms error between measured and the expected amplitude is 18 % of the max. amplitude. Thus, the number of distinguishable amplitude values that can

be generated with the presented holograms can be assumed to be five in the present setup.

In conclusion, we have demonstrated an efficient means of fabricating polarization holograms that control both amplitude and phase of the transmitted beam. The fabrication utilizes an SLM that is temporally modulated while it is imaged onto a photo-active polymer film. Our digital holograms and their generated amplitude and phase distributions are in good agreement with the predicted distributions. The fabrication process can be further improved by integrating a digital holographic read-out into the setup for writing the holograms, which would offer the possibility for real-time feedback and control during the write process. A number of applications suggest themselves, including the realization of 3D-displays [5] due to the ability to rewrite azobenzen-based photo-polymers.

References:
1. B. Brown, A. Lohmann, Appl. Opt. **5**, 967 (1966).
2. D. N. Christodoulides, Nature Photonics **2**, 652 (2008)
3. P. Polynkin, M. Kolesik, J. V. Moloney, G. A. Siviloglou, and D. N. Christodoulides, Science **324**, 229 (2009).
4. D. G. Grier, Nature **424**, 810 (2003).
5. S. Tay, P.-A. Blanche, R. Voorakaranam; A. V. Tunç, W. Lin, S. Rokutanda, T. Gu, D. Flores, P. Wang, G. Li, P. St Hilaire, J. Thomas, R. A. Norwood; M. Yamamoto, N. Peyghambarian, Nature **451**, 694 (2008).
6. D. Chu, J. Fienup, and J. Goodman, Appl. Opt. **12**, 1386 (1973).
7. T. Ando, Y. Ohtake, N. Matsumoto, T. Inoue, N. Fukuchi, Opt. Lett. **34**, 34 (2009).
8. V. Arrizón, G. Méndez, and D. Sánchez-de-La-Llave, Opt. Express **13**, 7913-7927 (2005).
9. H. Aagedal, M.Schmid, T. Beth, S. Teiwes, F. Wyrowski, R. Chaussee, J. Mod. Opt. 43, 1409 (1996).
10. M. Honkanen, V. Kettunen, J. Tervo, J. Turunen, J. Mod. Opt. **47,** 2351 (2000).
11. M. Fratz, D. Giel, P. Fischer, Opt. Lett. **34**, 1270 (2009).
12. L. Nikolova, P. S. Ramanujam, Cambridge University Press, New York (2009).
13. M. Fratz, S. Sinzinger, and D. Giel, Appl. Opt. **48**, 2669 (2009).
14. J. Eickmans, T. Bieringer, S. Kostromine, H. Berneth, R., Jpn. J. Appl. Ph. **38,** 1835 (1999).
15. J. Davis, D. McNamara, D. Cottrell, and T. Sonehara, Appl. Opt. **39**, 1549 (2000).
16. D. Carl, M. Fratz, M. Pfeifer, D. Giel, and H. Höfler, Appl. Opt. **48**, H1 (2009).